Exchange bias and magnetotransport properties in IrMn/NiFe/FeMn structures

Z. B. Guo,[1] Y. H. Wu,[2] J. J. Qiu,[1] B. Y. Zong,[1] and G. C. Han[1]
[1]*Data Storage Institute, Agency for Science, Technology and Research (A*STAR), DSI Building, 5 Engineering Drive 1, Singapore 117608*
[2]*Department of Electrical and Computer Engineering, National University of Singapore, Singapore 119260*
(Received 24 July 2008; revised manuscript received 7 October 2008; published 14 November 2008)

For the double exchange-biased IrMn/NiFe/FeMn structures, the pinning directions at IrMn/NiFe and NiFe/FeMn interfaces were set either parallel or antiparallel to each other by field annealing. Exchange bias and magnetotransport properties in IrMn/NiFe/FeMn trilayers were studied and compared with those of IrMn/NiFe and NiFe/FeMn bilayers. The dependence of exchange bias on the thickness of NiFe layer was different for parallel and antiparallel pinnings. A remarkable increase in resistance was observed which should be attributed to domain-wall resistance induced by the twisted spin structure. The spin configuration of twisted spin structure was simulated by one-dimensional atomic model.

DOI: 10.1103/PhysRevB.78.184413 PACS number(s): 75.30.Et, 75.60.Ch, 73.50.Jt

I. INTRODUCTION

Magnetic interlayer coupling and magnetotransport properties have attracted great interest in recent decades because of their intrinsic physics and important applications in magnetic information storage.[1–4] In which, the ferromagnetic/antiferromagnetic (FM/AFM) exchange coupling, inducing a shift of hysteresis loop away from zero-field axis—so-called exchange bias (H_{ex})—has been employed to pin the magnetization of the specific FM layer in magnetic read sensors and magnetic recording elements.[5,6] Magnetotransport is related to the change in resistance with respect to the magnetization direction and has been classified as anisotropic magnetoresistance (AMR),[7] giant magnetoresistance (GMR),[8] and domain-wall magnetoresistance,[9] etc.

A magnetic domain wall (DO) is an interface separating magnetic domains, where magnetic moments gradually reorientate, exhibiting a twisted spin structure. The magnetic domain-wall resistance (DR.) reflects the influence of forming twisted spin structures on electronic transport. Experimentally, DR. has been mainly studied in FM nanowires [e.g., Ni (Ref. 10) and Fe (Ref. 11)], films [e.g., Co (Ref. 12) and Fed (Ref. 13)], and patterned structures,[14,15] etc., where shape anisotropy, crystalline anisotropy, exchange bias, exchange spring, or combination of them have been used to obtain ordered Drys. Remarkably, both the increase and decrease in resistance with forming Drys have been observed; therefore, it is essential to achieve well-defined Drys so as to identify quantitatively the correlation between DR. and DO spin configuration. On the other hand, it is also important to achieve Drys as thin as possible because of the DO scattering inversely proportional to the squares of the DO thickness.[16] By using a NiFe/Gd/NiFe structure, DO magnetoresistance ~13% has been achieved in a constricted DO down to 4 nm.[17]

In this paper, we studied exchange bias and magnetotransport properties of a double exchange-biased structure of IrMn/NiFe/FeMn trilayers. Because of different Néel temperatures between IrMn and FeMn, the pinning directions could be set either parallel or antiparallel to each other and then due to the nature of interface interaction in FM/AFM system, twisted spin structures could be formed in the NiFe layer, resulting in different behaviors in exchange bias and magnetoresistance from those of exchange-biased bilayers.

II. EXPERIMENT, RESULTS, AND DISCUSSION

A. Sample fabrications

All films in this study were deposited at room temperature by magnetron sputtering on thermally oxidized Si (100) substrates under a magnetic field of 100 Oe. The base pressure of the system is 5×10^{-10} Torr. The structure of a series of double exchange bias samples consits of Ta(3 nm)/$Ni_{81}Fe_{19}$(2 nm)/$I_{20}Mn_{80}$(20 nm)/$Ni_{81}Fe_{19}$(t nm)/$Fe_{50}Mn_{50}$(20 nm)/Ta(3 nm) with t=5, 10, 20, 50, and 80, where the bottom Ta/NiFe acts as seed layers to promote (111) texture in the IrMn layer. For comparison, single exchange bias samples of IrMn/NiFe and NiFe/FeMn were also fabricated. To set a pinning direction, the samples were annealed in a vacuum oven with a magnetic field applied at the elevated temperatures and keeping the field on as the samples were cooled to room temperature. It is well known that the Néel temperature of IrMn (>900 °C) is much higher than that of FeMn (153 °C); therefore, for IrMn/NiFe/FeMn structures, if annealing at a high temperature with a field along the field applied during film deposition (defined as positive field), the exchange bias directions in IrMn/NiFe and NiFe/FeMn should be parallel. After that if the sample is further annealed in a temperature lower than the Néel temperature of IrMn but higher than that of FeMn with a field opposite to the direction of the field applied during film deposition (defined as negative field), the pinning direction in NiFe/FeMn should be reversed, while the pinning direction in IrMn/NiFe should be unaffected, which results in antiparallel pinning.

B. Exchange bias

Figures 1(a) and 1(b) show the effect of annealing on the pinning directions in IrMn(20 nm)/NiFe(10 nm) and NiFe(10 nm)/FeMn(20 nm) bilayers based on the above-specified annealing procedure. After annealing at 250 °C for 1 h under a

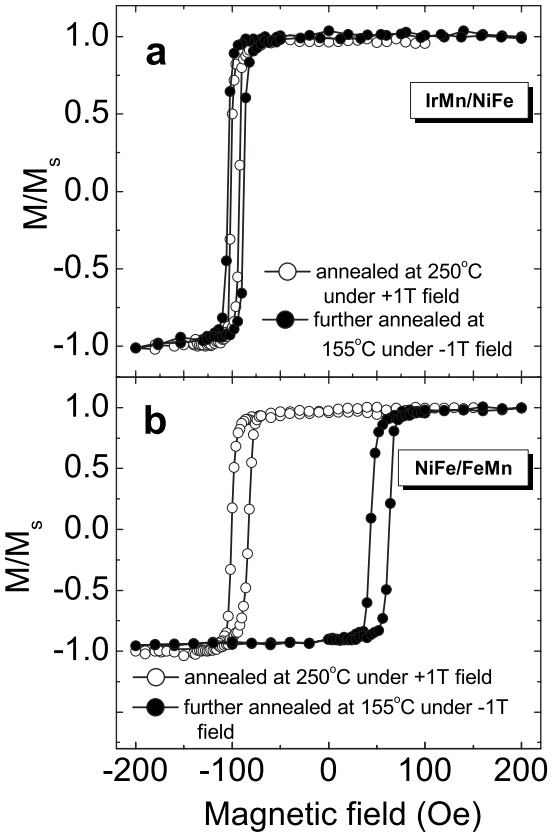

FIG. 1. (a) and (b) are the hysteresis curves of IrMn/NiFe and NiFe/FeMn bilayers after annealing at 250 °C (open symbols) under a field of +1 T and then further annealing at 155 °C under a field of −1 T (solid symbols).

field of +1 T, H_{ex} is −96 and −92 Oe for IrMn/NiFe and NiFe/FeMn, respectively. The samples were then annealed further at 155 °C for 1 h under a field of −1 T. This temperature is a little bit higher than the Néel temperature of FeMn (153 °C) but much lower than the Néel temperature of IrMn (>900 °C). After the annealing, the pinning direction in NiFe/FeMn was reversed and H_{ex} is ~54 Oe [Fig. 1(b)], while the magnitude of $|H_{ex}|$ and the pinning direction in IrMn/NiFe were no obvious changes. [Fig. 1(a)] It is deserving to note that the pinning direction in NiFe/FeMn can also be reversed at temperatures higher than 155 °C, but in this case, the disadvantage is that it would weaken the exchange bias in IrMn/NiFe. For example, annealing IrMn/NiFe at 250 °C under −1 T field results in $H_{ex}\sim-46$ Oe, i.e., $|H_{ex}|$ decreases ~50% from $H_{ex}\sim-96$ Oe.

It could be expected from the above results that for the double exchange-biased IrMn/NiFe/FeMn structures, the pinning directions at NiFe/FeMn and IrMn/NiFe interfaces could be set either parallel to each other by annealing at 250 °C under a field of +1 T or antiparallel to each other by further annealing at 155 °C under a field of −1 T. Shown in Figs. 2(a) and 2(b) are the diagrams of the magnetization configurations in a IrMn/NiFe/FeMn structure with parallel and antiparallel pinnings, respectively. At $H=0$, magnetization is saturated when the pinning directions are parallel and a reversal field should induce the magnetic-moment rotation, thus leading to a twisted spin structure [Fig. 2(a)]. However,

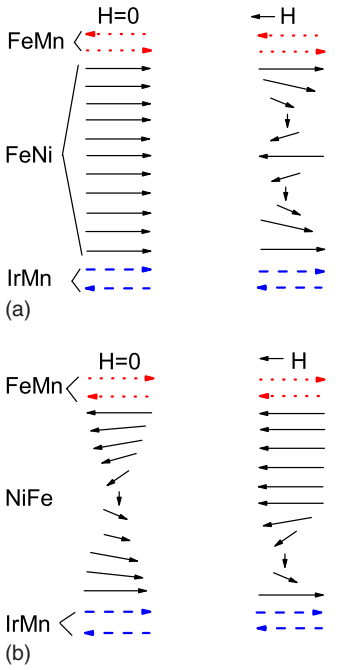

FIG. 2. (Color online) (a) and (b) are the magnetization configurations and reversal in IrMn/NiFe/FeMn structure with parallel and antiparallel pinning directions, respectively.

for the sample with antiparallel pinning, a twisted spin structure should be present at $H=0$ and an applied field should compress it toward a FM/AFM interface [Fig. 2(b)].

It is well known that for FM/AFM bilayers, the magnitude of H_{ex} is given by

$$|H_{ex}| = J/(M_F t_F), \tag{1}$$

where J is the FM-AFM interfacial exchange coupling energy, M_F is the magnetization per unit volume, and t_F is the thickness of the ferromagnetic layer.[18] Since J and M_F are constants, H_{ex} would be reversely proportional to t_F; this relation has been confirmed extensively in experiments.[19,20] Substituting $M_F=800$ emu/cm^3, $|H_{ex}|=96$, and 92 Oe, $J\sim0.077$ and 0.074 erg/cm^2 were obtained for IrMn/NiFe and NiFe/FeMn bilayers, respectively.

Shown in Figs. 3(a) and 3(b) are the hysteresis loops of IrMn(20 nm)/NiFe(t nm)/FeMn(20 nm) samples with parallel and antiparallel pinnings, respectively, and the insets of Fig. 3 are the exchange bias as a function of the thickness of NiFe layer. For the samples with parallel pinning, H_{ex} well fits Eq. (1) with $J=0.163$ erg/cm^2; the magnitude of J is very close to the sum of J from IrMn/NiFe ($J=0.077$ erg/cm^2) and NiFe/FeMn ($J=0.074$ erg/cm^2), this result is in good agreement with the previous reports.[21,22] However, for the samples with antiparallel pinning, the dependence of H_{ex} on t_F fits the form of $|H_{ex}|=J/(M_F t_F^b)$ with $J=0.008$ erg/cm^2 and $b=1.3$, which is different from that of FM/AFM bilayers and IrMn/NiFe/FeMn trilayers with parallel pinning, indicating that the presence of the twisted spin structure at zero field should play a role in magnetization reversal thus affecting H_{ex} dependence on t_F [Fig. 2(b)].

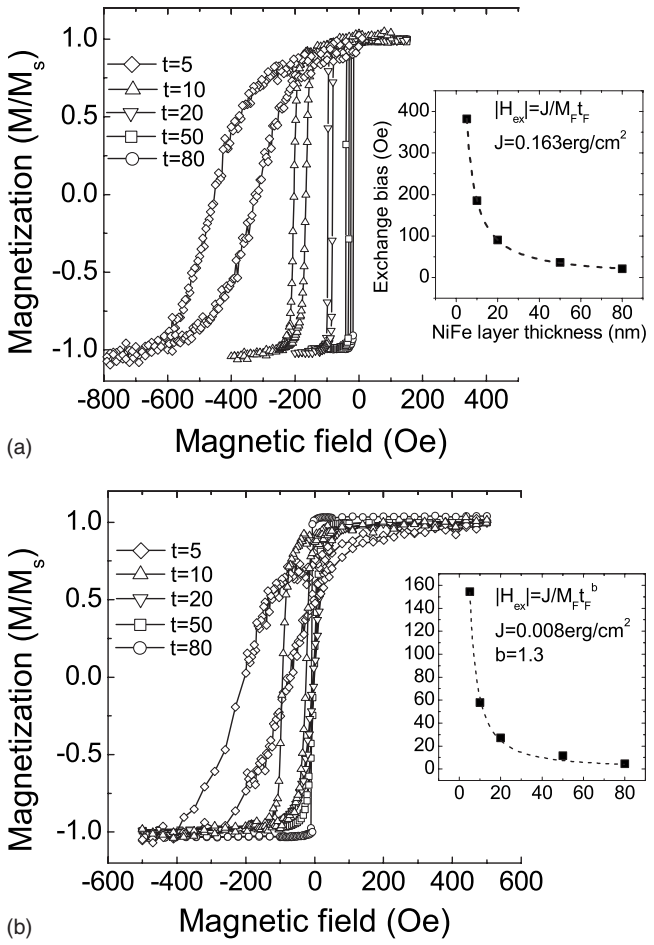

FIG. 3. (a) The hysteresis loops of IrMn(20 nm)/NiFe(t nm)/FeMn(20 nm) with $t=5$, 10, 20, 50, and 80 after annealing at 250 °C under a field of +1 T and (b) after further annealing at 155 °C under a field of −1 T. Insets are exchange bias as a function of NiFe layer thickness. Dashed lines are fitting curves.

C. One-dimensional atomic model

To illustrate the spin configurations in the IrMn/NiFe/FeMn structure, a one-dimensional atomic model is proposed: this model is extended from that for exchange spring bilayers.[14,23] For the AFM1/FM/AFM2 system, the total energy E is given by

$$E = -\sum_{i=1}^{n-1} \frac{A_{\mathrm{AF1}}}{d_{\mathrm{AF1}}^2}\cos(\theta_i - \theta_{i+1}) + \sum_{i=1}^{n} K_{\mathrm{AF1}} \sin^2\theta_i - \frac{J_1}{d_{\mathrm{F}}^2}\cos(\theta_n - \theta_{n+1}) - \sum_{i=n+1}^{m-1} \frac{A_{\mathrm{F}}}{d_{\mathrm{F}}^2}\cos(\theta_i - \theta_{i+1}) + \sum_{i=n+1}^{m} K_{\mathrm{F}} \sin^2\theta - \sum_{i=n+1}^{m} HM_i \cos(\theta_i - \theta_H) - \frac{J_2}{d_{\mathrm{F}}^2}\cos(\theta_m - \theta_{m+1}) - \sum_{i=m+1}^{m'-1} \frac{A_{\mathrm{AF2}}}{d_{\mathrm{AF2}}^2}\cos(\theta_i - \theta_{i+1}) + \sum_{i=m+1}^{m'} K_{\mathrm{AF2}} \sin^2\theta_i. \quad (2)$$

Here the index $i=1$ through n corresponds to the AFM1 layer with magnetization anisotropy K_{AF1}, exchange coupling constant A_{AF1}, and adjacent spin distance d_{AF1}. J_1 is the AFM1/FM interface exchange constant. The index $i=n+1$ through m corresponds to the FM layer with magnetization anisotropy K_{F}, exchange coupling constant A_{F}, and adjacent spin distance d_{F}. J_2 is the FM/AFM2 interface exchange constant. The index $i=m+1$ through m' corresponds to the AFM2 layer with magnetization anisotropy K_{AF2}, exchange coupling constant A_{AF2}, and adjacent spin distance d_{AF2}. θ_i is the angle between the ith atomic spin and easy axis and θ_H is the angle between the external field and easy axis. In Eq. (2) the first two terms are exchange and anisotropy energies in the AFM1 layer, respectively. The third term is exchange energy between the AFM1 and the FM layers at the interface. The fourth, fifth, and sixth terms are exchange, anisotropy, and Zeeman energies in the FM layer, respectively. The seventh term is exchange energy between the FM layer and the AFM2 layer at the interface. The eighth and ninth terms are exchange energy and anisotropy energies in the AFM2 layer, respectively.

The spin configurations in the IrMn/NiFe/FeMn trilayers are obtained by iteration method with the parameters of $A_{\mathrm{IrMn}}=-3.27\times10^{-7}$ erg/cm and $A_{\mathrm{FeMn}}=-3.0\times10^{-7}$ erg/cm for annealing at a field of +1 T, and $A_{\mathrm{FeMn}}=-1.03\times10^{-7}$ erg/cm for further annealing at a field of −1 T, $d_{\mathrm{NiFe}}=d_{\mathrm{IrMn}}=d_{\mathrm{FeMn}}=2$ Å, $A_{\mathrm{IrMn}}=-3.27\times10^{-7}$ erg/cm, $K_{\mathrm{IrMn}}\approx K_{\mathrm{FeMn}}=1.3\times10^5$ erg/cm^3,[24] $A_{\mathrm{NiFe}}=1.0\times10^{-8}$ erg/cm, $J_1=|A_{\mathrm{IrMn}}|$, $J_2=|A_{\mathrm{FeMn}}|$, $K_{\mathrm{NiFe}}=1.0\times10^3$ erg/cm^3, $M=800$ emu/cm^3,[25] and $\theta_H=0$. Shown in Fig. 4 is the representative spin configurations of IrMn(20 nm)/NiFe(t nm)/FeMn(20 nm) with $t=5$ and 50, where only one of the AFM sublattices is present. For the samples with parallel pinning [Figs. 4(a) and 4(c)], magnetization is saturated at zero field by the pinning field and the reversal field induces a twisted spin structure. However, for the samples with antiparallel pinning direction [Figs. 4(b) and 4(d)], as the applied field decreases, a twisted spin structure is formed throughout the thickness of NiFe layer and then it is compressed toward the FM/AFM interface whose pinning direction is antiparallel to the applied field, also illustrated in Fig. 2(b).

D. Transport properties

Krivorotov *et al.* studied the electrical transport in an AFM/FM/AFM trilayer under a rotation field, where the FM film is a colossal magnetoresistance material $La_{2/3}Ca_{1/3}(Sr_{1/3})MnO_3$.[26] In this paper, transport properties measurement was performed by four-point probe method with current-in-plane geometry and with both current and magnetic fields along the pinning direction. In this measurement, both DR. and AMR effects contribute to magnetoresistance. Shown in the left and right panels of Fig. 5 are the representative dependences of resistance on the field in the IrMn(20 nm)/NiFe(t nm)/FeMn(20 nm) samples with parallel and antiparallel pinnings, respectively. For $t=5$, resistance increases with decreasing field and presents a peak around the coercive field [Figs. 5(a) and 5(b)]. On the contrary, for $t\geq10$, resistance first decreases with decreasing field from saturation followed by a sharp increase. The magnetotrans-

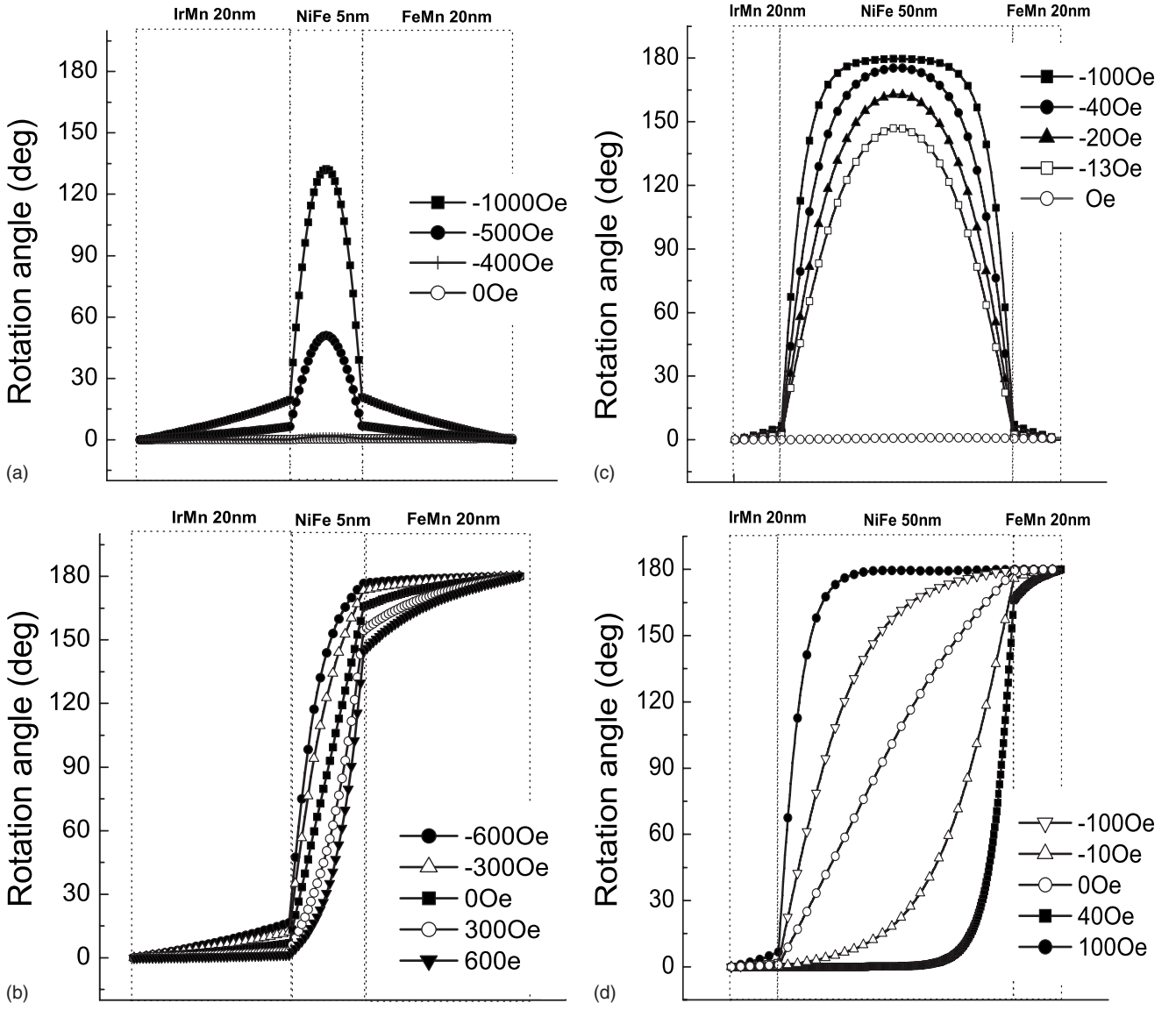

FIG. 4. (a) and (b) are the magnetization configurations of IrMn(20 nm)/NiFe (5 nm)/FeMn(20 nm) with parallel and antiparallel pinning directions, respectively. (c) and (d) are the magnetization configurations of IrMn(20 nm)/NiFe(50 nm)/FeMn(20 nm) with parallel and antiparallel pinning directions, respectively. The figures show layer by layer magnetization projections onto the plane of the paper.

port characteristics of these samples are remarkably different from those of FM/AFM bilayers. For comparison, shown in Fig. 6 is the dependence of resistance on the field in IrMn/NiFe and NiFe/FeMn bilayers, which is in agreement with the previous reports, i.e., resistance decreases as decreasing field, and then reaches a minimum near the coercive field. This phenomenon has been attributed to the AMR effect.[27,28] For FM/AFM bilayers, magnetization reversal is dominated by nucleation and domain-wall movement, which is similar to that of a FM single layer, and leads to the presence of AMR-type magnetoresistance. The magnetization reversal in FM/AFM bilayers is asymmetric, resulting in an asymmetric hysteresis loop, while it is usually symmetric in a FM single layer.[28–30]

To the best of our knowledge, the magnetization reversal in double exchange-biased films, in particular of the structure like the present IrMn/NiFe/FeMn with parallel or antiparallel pinning directions has not been extensively studied yet. Although the one-dimensional atomic model could not reflect exactly the reversal behavior in the film system, the twisted spin structure shown in Fig. 4 is most possibly localized due to the random distribution of local magnetization in the polycrystalline AFM layers,[18,31] which could be used to explain the increase in resistance as follows. For samples with a thin NiFe layer, i.e., $t \leq 5$, as the magnetization at both the top and bottom surfaces of NiFe layer is pinned antiparallelly by the respective AFM layers, a twisted spin structure, such as a DO with DO thickness equal to the thickness of NiFe layer, is induced [Fig. 4(b)]; this structure is similar to that of the Gd layer in NiFe/Gd/NiFe.[17] On the other hand, for the samples with parallel pinning direction, the twisted spin structure could be formed when a certain reversal field is applied [Fig. 4(a)]. The small DO thickness in these samples would induce the magnetoresistance to be dominated by DO

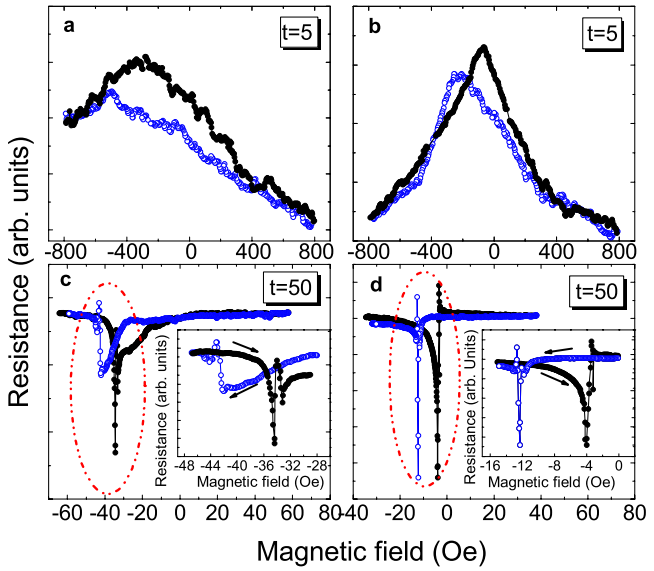

FIG. 5. (Color online) Magnetoresistance curves of IrMn(20 nm)/NiFe(t nm)/FeMn(20 nm). (a) and (b) are for $t=5$ with parallel and antiparallel pinning directions, respectively. (c) and (d) are for $t=50$ for parallel and antiparallel pinning directions, respectively. Solid and open symbols are for the field scans from negative to positive and from positive to negative, respectively. The insets are the enlarged views.

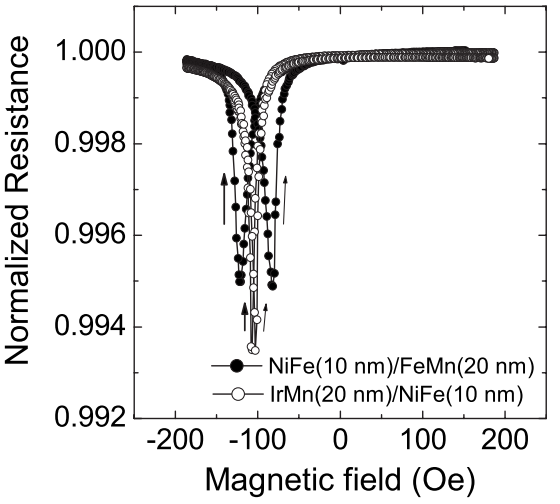

FIG. 6. Magnetoresistance curves of IrMn(20 nm)/NiFe(10 nm), and NiFe(10 nm)/FeMn(20 nm) bilayers.

scattering, exhibiting an increase in resistance with decreasing the applied field from magnetization saturation. For the samples with a thick NiFe layer, i.e., $t>10$ [Figs. 5(c) and 5(d)], resistance decreases with decreasing field, which should be due to the AMR effect, and then sharply increases due to the DO scattering.

Different from the AMR-type magnetotransport in FM/AFM bilayers, the remarkable characteristic in the magnetotransport properties in IrMn/NiFe/FeMn trilayers is the presence of increase in resistance attributed to the twisted spin structure which likes a DO. This phenomenon indicates that the AFM/FM/AFM structure is potentially a very suitable platform for DR. studies with the advantages of (i) thin and controllable DO thickness, as the DO thickness could be exactly the same as the FM film thickness, (ii) avoidance of the GMR effect which presents in the NiFe/Gd/NiFe structure by using AFM layers as the pinning layers,[17] and (iii) achieving various DO angles by controlling the angle between the pinning directions.

III. CONCLUSIONS

In summary, the present study demonstrates that for the double exchange-biased IrMn/NiFe/FeMn structures, due to the different Néel temperatures of IrMn and FeMn, the pinning directions at IrMn/NiFe and NiFe/FeMn interfaces could be set either parallel or antiparallel to each other by field annealing, which results in the formation of a twisted spin structure in magnetization reversal, and then leads to the observation of different characteristics in exchange bias and magnetoresistance. The advantages of this kind of structure for domain-wall resistance study have been discussed.

ACKNOWLEDGMENTS

The authors would like to thank S. Zhang, K. B. Li, and Y. K. Zheng for valuable discussions.

[1] A. Fert, P. Grünberg, A. Barthélémy, F. Petroff, and W. Zinn, J. Magn. Magn. Mater. **140-144**, 1 (1995).
[2] M. D. Stiles, J. Magn. Magn. Mater. **200**, 322 (1999).
[3] M. N. Baibich, J. M. Broto, A. Fert, F. Nguyen Van Dau, F. Petroff, P. Etienne, G. Creuzet, A. Friederich, and J. Chazelas, Phys. Rev. Lett. **61**, 2472 (1988).
[4] K. B. Li, Y. H. Wu, Z. B. Guo, Y. K. Zheng, G. C. Han, J. J. Qiu, P. Luo, L. H. An, and T. J. Zhou, J. Nanosci. Nanotechnol. **7**, 13 (2007).
[5] C. Tsang and R. Fontana, IEEE Trans. Magn. **18**, 1149 (1982).
[6] B. N. Engel, J. Åkerman, B. Butcher, R. W. Dave, M. DeHerrera, M. Durlam, G. Grynkewich, J. Janesky, S. V. Pietambaram, N. D. Rizzo, J. M. Slaughter, K. Smith, J. J. Sun, and S. Tehrani, IEEE Trans. Magn. **41**, 132 (2005).
[7] I. A. Campbell and A. Fert, in *Ferromagnetic Materials*, edited by E. P. Wolfarth (Elsevier, Amsterdam, 1982), Vol. 3, p. 747.
[8] G. Binasch, P. Grünberg, F. Saurenbach, and W. Zinn, Phys. Rev. B **39**, 4828 (1989).
[9] M. Viret, D. Vignoles, D. Cole, J. M. D. Coey, W. Allen, D. S. Daniel, and J. F. Gregg, Phys. Rev. B **53**, 8464 (1996).
[10] K. Hong and N. Giordano, J. Phys.: Condens. Matter **10**, L401 (1998).
[11] U. Ruediger, J. Yu, S. Zhang, A. D. Kent, and S. S. P. Parkin, Phys. Rev. Lett. **80**, 5639 (1998).
[12] J. F. Gregg, W. Allen, K. Ounadjela, M. Viret, M. Hehn, S. M. Thompson, and J. M. D. Coey, Phys. Rev. Lett. **77**, 1580

(1996).
[13] D. Ravelosona, A. Cebollada, F. Briones, C. Diaz-Paniagua, M. A. Hidalgo, and F. Batallan, Phys. Rev. B **59**, 4322 (1999).
[14] K. Mibu, T. Nagahama, T. Shinjo, and T. Ono, Phys. Rev. B **58**, 6442 (1998).
[15] D. Buntinx, S. Brems, A. Volodin, K. Temst, and C. Van Haesendonck, Phys. Rev. Lett. **94**, 017204 (2005).
[16] P. M. Levy and S. Zhang, Phys. Rev. Lett. **79**, 5110 (1997).
[17] J. L. Prieto, M. G. Blamire, and J. E. Evetts, Phys. Rev. Lett. **90**, 027201 (2003).
[18] A. P. Malozemoff, Phys. Rev. B **35**, 3679 (1987).
[19] D. Mauri, E. Kay, D. Scholl, and J. K. Howard, J. Appl. Phys. **62**, 2929 (1987).
[20] J. Nogués and I. K. Schuller, J. Magn. Magn. Mater. **192**, 203 (1999).
[21] B. Viala, G. Visentin, and P. Gaud, IEEE Trans. Magn. **40**, 1996 (2004).
[22] J. Sort, B. Dieny, and J. Nogués, Phys. Rev. B **72**, 104412 (2005).
[23] E. E. Fullerton, J. S. Jiang, M. Grimsditch, C. H. Sowers, and S. D. Bader, Phys. Rev. B **58**, 12193 (1998).
[24] D. Mauri, H. C. Siegmann, P. S. Bagus, and E. Kay, J. Appl. Phys. **62**, 3047 (1987); $A_{\mathrm{FeMn}}=-3.0\times10^{-7}$ erg/cm is cited from the reference and then $A_{\mathrm{FeMn}}=-1.03\times10^{-7}$ for annealing under a field of -1 T and $A_{\mathrm{IrMn}}=-3.27\times10^{-7}$ erg/cm are obtained from the relation of $|H_{\mathrm{ex}}|\propto(|A_{\mathrm{AF}}|)^{1/2}$.
[25] M. R. Gibbons, J. Magn. Magn. Mater. **186**, 389 (1998).
[26] I. N. Krivorotov, K. R. Nikolaev, A. Y. Dobin, A. M. Goldman, and E. D. Dahlberg, Phys. Rev. Lett. **86**, 5779 (2001).
[27] B. H. Miller and E. D. Dahlberg, Appl. Phys. Lett. **69**, 3932 (1996).
[28] M. Gruyters, J. Appl. Phys. **95**, 2587 (2004).
[29] C. Leighton, M. R. Fitzsimmons, P. Yashar, A. Hoffmann, J. Nogués, J. Dura, C. F. Majkrzak, and I. K. Schuller, Phys. Rev. Lett. **86**, 4394 (2001).
[30] T. Gredig, I. N. Krivorotov, and E. D. Dahlberg, J. Appl. Phys. **91**, 7760 (2002).
[31] U. Nowak, K. D. Usadel, J. Keller, P. Miltényi, B. Beschoten, and G. Güntherodt, Phys. Rev. B **66**, 014430 (2002).